RETRACTION
https://doi.org/10.1071/CH18641_RE

AUSTRALIAN JOURNAL OF CHEMISTRY

Retraction notice to 'Three Cu^{II} and Co^{II} coordination complexes containing tridentate schiff base moieties induce ROS generation and lead to caspase-dependent apoptotic cell death in intracranial aneurysm'

Hui Li and Zhi-Yuan Hu

Australian Journal of Chemistry (2019)
doi.org/10.1071/CH18641

Refers to: RETRACTED: Three Cu^{II} and Co^{II} Coordination Complexes Containing Tridentate Schiff Base Moieties Induce ROS Generation and Lead to Caspase-Dependent Apoptotic Cell Death in Intracranial Aneurysm, published 12 April 2019, doi.org/10.1071/CH18641. Hui Li and Zhi-Yuan Hu.

After due consideration of issues raised with respect to this paper, the Editors-in-Chief and the authors agree to retract the paper from *Australian Journal of Chemistry*. Reason: Upon review of the submission history for the manuscript, the *Australian Journal of Chemistry* Editors and Publisher found indications that the peer review process is likely to have been compromised by the submission of reviews through suspected fabricated reviewer accounts.

The Editors-in-Chief and Journal Publisher have determined these are grounds for retraction, according to the international guidelines established by the Committee on Publication Ethics. We regret the academic record was compromised and apologise for any inconvenience this may have caused.

Li H and Hu Z-Y (2023) *Australian Journal of Chemistry*,
76(9), 631. doi:10.1071/CH18641_RE

CSIRO PUBLISHING

Aust. J. Chem.
https://doi.org/10.1071/CH18641

Full Paper

Three Cu^{II} and Co^{II} Coordination Complexes Containing Tridentate Schiff Base Moieties Induce ROS Generation and Lead to Caspase-Dependent Apoptotic Cell Death in Intracranial Aneurysm

Hui Li[A] *and Zhi-Yuan Hu*[A,B]

[A]Department of Neurosurgery, Zhangye People's Hospital of HeXi College, Zhangye, Gansu 734000, China.
[B]Corresponding author. Email: zhiyuan_hu666@126.com

Two similar tridentate Schiff base ligands with N,O,O-donor sites, 2-methoxy-6-(((2-(piperazin-1-yl)ethyl)amino)methyl)phenol (HL_1) and 2-(((2-(dimethylamino)ethyl)amino)methyl)-6-methoxyphenol (HL_2) have been synthesised by a one pot condensation reaction, and were further used in the construction of three novel Schiff base Cu^{II} and Co^{II} coordination complexes $[Cu(L_1)(OAc)]$ (**1**), $[Co(L_2)(OAc)]$ (**2**), and $[Cu(L_2)(N_3)(CH_3OH)]$ (**3**). Furthermore, the particle sizes of these coordination complexes have been successfully reduced to the nano-region via a hand grinding method. In addition, the anti-proliferation activity of nano **1–3** was detected on human intracranial aneurysm SF767 cells with a Cell Counting Kit-8 assay. The half maximal inhibitory concentration values calculated from the cell viability curves indicated that only nano **1** has anti-proliferation activity on SF767 cells. To further investigate the anticancer mechanism of nano **1**, a Western blot assay, reactive oxygen species level detection, and an Annexin V-FITC/PI double staining assay were conducted.

Manuscript received: 30 December 2018.
Manuscript accepted: 15 March 2019.
Published online: 12 April 2019.

Introduction

Cancer is a great threat to the health of human beings and causes millions of deaths every year both in the developing and undeveloped countries.[1] Saccular unruptured intracranial aneurysms (UIAs) occur in ~[illegible] of the adult population, and due to the speed of cranial imaging with improved quality, it could be easily detected, to allow ample time for patients' treatment.[2,3] To give more [illegible] to cancer patients as well as to reduce the mortality rate of cancer, chemists and biologist have devoted considerable efforts to developing new anticancer reagents based on natural or synthetic compounds for treating cancer with improved efficacy and less toxicity. Among the synthetic compounds for anticancer activity evaluation, metal-based compounds formed by chelating an organic ligand with a metal ion via coordination bonds have drawn the attention of scientists all over the world since the discovery and success of the famous anticancer drug cisplatin and its analogues, it still being one of the best-selling and effective anticancer drugs to date. However, cisplatin and its analogues have some drawbacks, especially their severe side effects, which can result in damage to normal human tissues and therefore limits their large dose of administration.[4,5] Metal–organic complexes based on less toxic elements such as Cu^{II} and Co^{II} have been constructed for the purpose of addressing the clinical problems of platinum-based anticancer drugs.

The coordination complexes constructed from the transition metal elements along with multidentate heterocyclic ligands have undergone booming development in the last few decades not only for their diversiform architectures but also for their promising biological activities which could be used in the fields of anticancer and antisepsis.[6] Coordination compounds, especially those constructed from the Schiff base ligands bearing sp^2 hybrid N atoms, have important applications as anticancer drugs.[7] The use of Schiff base ligands in the construction of coordination complexes could not only afford new complexes with diversiform structural features but could also result in complexes with important pharmacological properties.[8] The recent literature has revealed that Co^{II} and Cu^{II}-based Schiff base compounds show promising anticancer activities.[9–11] For instance, Natarajan and co-workers developed a Co^{II}-based coordination polymer by use of a dihydroquinoline-type ligand, which showed substantial anticancer activity against a series of cancer cells.[8] Sukanya et al. have obtained a Cu^{II} based coordination complex based on a quinoxalin-type Schiff base ligand, which showed promising cytotoxicity and growth inhibition effect towards the B16-F10, HeLa, and MCF-7 cancer cell lines.[6] To study the metal and ligand effects in the anticancer activities of the Schiff base metal complexes, in this study, two similar tridentate Schiff base ligands with N,O,O-donor sites, 2-methoxy-6-(((2-(piperazin-1-yl)ethyl)amino)methyl)phenol (HL_1) and 2-(((2-(dimethylamino)ethyl)amino)methyl)-6-methoxyphenol (HL_2) have been synthesised by a one pot condensation reaction, and were further used in the construction of three novel trinuclear Schiff base Cu^{II} and Co^{II} coordination

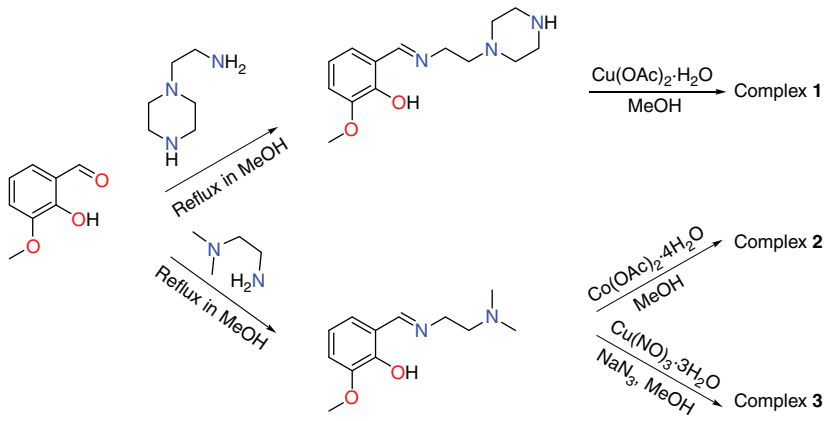

Scheme 1. Synthetic routes to the title complexes **1**–**3**.

complexes [Cu(L_1)(OAc)] (**1**), [Co(L_2)(OAc)] (**2**), and [Cu(L_2)(N_3)(MeOH)] (**3**) (Scheme 1). The as-prepared complexes were characterised using various physicochemical techniques, e.g. power X-ray diffraction (PXRD), X-ray single crystal diffraction (SCXRD), elemental analyses (EA), and thermogravimetric analysis (TGA). Furthermore, the particle sizes of coordination complexes **1**–**3** have been reduced to the nano-region via a hand grinding method. To investigate their anticancer activity and mechanism, we first evaluated the anti-proliferation activity of nano **1**–**3** on human intracranial aneurysm SF767 cells. Both the cell viability curves and half maximal inhibitory concentration (IC_{50}) values suggested that only nano **1** exhibits anticancer activity and has no cytotoxicity on HEK-293 normal human cells. Western blot results and an Annexin V-FITC/PI assay confirmed that nano **1** exerts anti-proliferation activity due to the induction of apoptotic cancer cell death. In a further study, we confirmed that nano **1** could initiate reactive oxygen species (ROS) generation in SF767 cells, and finally lead to the production of caspase-dependent apoptotic cell death.

Experimental

Measurements and Reagents

PXRD profiles were collected on a MiniFLEX XRD diffractometer (D/Max 2500 V, made in Japan) using Cu Kα radiation, and the electric current and voltage were 40 mA and 40 kV. Scanning electron microscopy (SEM) was carried out using a Hitachi S4800 electron microscope. The elemental content percentage of H, C, and N were acquired using a PerkinElmer 240 elemental analyser. TGA was performed over a temperature range of 25–800°C using a PerkinElmer Pyris 1. All the starting materials, solvents, and metal salts were obtained from the Beijing Bailingwei Reagent company and were of analytical grade.

*Synthesis of Compounds **1**–**3***

$Cu(OAc)_2{\cdot}H_2O$ (199 mg, 1 mmol) and the ligand HL_1 (263 mg, 1 mmol) were separately dissolved in 10 mL of MeOH via stirring or ultrasonic processing. The two solutions were then mixed and refluxed for ~30 min. The final solution was refluxed for an additional hour after the addition of a MeOH/H_2O solution (9 mL, v/v, 2 : 1) containing AcONa (2 mmol, 164 mg). After slow evaporation of the solution in air for one week, blue block-shaped crystalline crystals of **1** were obtained by filtration, cleaned by MeOH, and dried in the air (yield: ~62 % based on copper (II)). Anal. Calc. for $C_{16}H_{22}CuN_3O_4$: N 10.95, H 5.78, C 50.06. Found: N 10.45, H 5.62, C 49.91 %.

$Co(OAc)_2{\cdot}4H_2O$ (177 mg, 1 mmol) and the ligand HL_2 (333 mg, 1.5 mmol) were separately dissolved in 10 mL of MeOH via stirring or ultrasonic processing. The two solutions were then mixed and refluxed for ~30 min. The solution was refluxed for an additional hour after the addition of a MeOH/H_2O solution (9 mL, v/v, 2 : 1) containing AcONa (2 mmol, 164 mg). After slow evaporation of the solution in air for one week, pink rod-like crystals of **2** were obtained by filtration, washed with MeOH, and dried in the air (yield: ~48 % based on $Co(OAc)_2{\cdot}4H_2O$). Anal. Calc. for $C_{14}H_{20}CoN_2O_4$: N 8.26, C 49.27, H 5.94. Found: N 8.45, C 49.91, H 5.62 %.

$Cu(NO)_3{\cdot}3H_2O$ (240 mg, 1 mmol) and the ligand HL_2 (333 mg, 1.5 mmol) were separately dissolved in 10 mL of MeOH via stirring or ultrasonic processing. The two solutions were then mixed and refluxed for ~30 min. The solution was refluxed for further ~30 min after the addition of 10 mL of MeOH containing sodium azide (130 mg, 2 mmol). After slow evaporation of the solution in air for one week, pink rod-like crystals of **3** were obtained by filtration, washed with MeOH, and dried in the air (yield: ~54 % based on Cu). Anal. Calc. for $C_{13}H_{20}CuN_5O_3$: C 43.63, H 5.63, N 19.57. Found: C 43.12, H 5.66, N 19.39 %.

X-Ray Data Collection and Refinements

The intensity data for complexes **1**–**3** were acquired using an Oxford Xcalibur E diffractometer with graphite monochromated Mo Kα radiation at room temperature. The raw data collected were reduced to *HKL* and *P4P* files using the *CrysAlisPro* software based on the computer-controlled procedure. The *XPREP* program was used to generate the *INS* file which was used in the following structural solution and refinement process. The structural solution was performed using the *SHELXS* program based on direct methods and then the obtained structural model was refined using the *SHELXL* program embedded in the *SHELXL-2014* software package. All the H atoms were generated on their attached atoms using the AFIX commands and all non-H atoms were refined based on thermal vibration parameters. Table 1 shows the refinement indexes for the three complexes.

Cell Lines and Cell Culture

The human intracranial aneurysm SF767 cells and normal human embryonic kidney cells HEK-293 were purchased from ATCC (American Type Culture Collection). The SF767 cancer cells were cultured in ATCC-formulated Leibovitz's L-15

Table 1. Structural refinement indexes for 1–3

Parameter	1	2	3
Empirical formula	$C_{16}H_{23}CuN_3O_4$	$C_{14}H_{20}CoN_2O_4$	$C_{13}H_{20}CuN_5O_3$
Formula weight	384.91	339.25	357.88
Temperature [K]	273.15	293(2)	296.15
Crystal system	monoclinic	orthorhombic	triclinic
Space group	*C*2/*c*	*Pbca*	*P*-1
a [Å]	14.9863(3)	8.263(3)	8.7103(3)
b [Å]	12.5593(4)	16.956(4)	9.8314(3)
c [Å]	20.1308(6)	21.468(9)	10.9631(4)
α [deg.]	90	90	99.028(2)
β [deg.]	91.762(2)	90	108.702(2)
γ [deg.]	90	90	108.033(2)
Volume [$Å^3$]	3787.18(18)	3007.9(18)	810.64(5)
Z	8	8	2
ρ_{calc} [g cm^{-3}]	1.350	1.498	1.466
μ [mm^{-1}]	1.176	1.158	1.366
Radiation	MoKα (λ 0.71073)	MoKα (λ 0.71[illegible])	MoKα (λ 0.71073)
2θ range for data collection [deg.]	4.048 to 55.202	6.124 to [illegible]9.376	4.092 to 50.048
Goodness-of-fit on F^2	1.104	[illegible].081	1.089
Final R indexes [$I \geq 2\sigma(I)$]	R_1 0.0587	[illegible]0.05[illegible]5	R_1 0.0523
	ωR_2 0.1881	ωR_2 [illegible]416	ωR_2 0.1683
Final R indexes [all data]	R_1 0.0700	R_1 0.[illegible]	R_1 0.0560
	ωR_2 0.1973	ωR_2 0.19[illegible]	ωR_2 0.1714
Largest diff. peak/hole [e $Å^{-3}$]	0.95/−0.68	[illegible]0.67/−0.72	0.78/−0.80
CCDC	1896855	[illegible]896856	1896857

medium. The HEK-293 cell line was cultured in DMEM (Dulbecco's modified Eagle's medium). Both culture mediu[illegible] contain 100 U mL^{-1} penicillin and streptomycin solutio[illegible] (GIBCO BRL Life Technologies), 10 % (v/v) heat[illegible]ctivated fetal bovine serum (FBS) (HyClone, Logan, UT, USA) [illegible]nd 2 % L-glutamine. The cells were cultured in a humidi[illegible] at[illegible]e of 5 % CO_2 with 95 % air.

Cell Counting Kit-8 (CCK-8) Assay

After treatment with nano **1–3**, t[illegible] proliferati[illegible]d viability of SF767 and HEK-293 cells w[illegible]e assessed using a CCK-8 assay following the manufacturer s[illegible]ols.[13] In brief, the SF767 and HEK-293 cells were seeded [illegible]-wel[illegible] plates at a concentration of 5 × 10^5 cells w[illegible]ll [illegible]d grew [illegible] confluence of 70–80 % at 37°C under 5 % C[illegible]mid[illegible]d atmosphere. Next, the cells were incubated with a serie[illegible] concentrations of nano **1–3** (1, 2, 4, 8, 10, 20, 40, 80, and 100 μ[illegible] 24 h at 37°C under 5 % CO_2. After incubation, the cells wer[illegible] harvested with 1 × trypsin-EDTA (5 min, 37°C) and centrifuged at 1120 *g* for 5 min. The medium was discarded, and 100 μL of 10 % CCK-8 in medium without FBS was added into wells for 2 h incubation at 37°C in the dark. A Thermo Scientific Microplate Reader was then used to measure the absorbance of each well at 450 nm. The cell viability curves were calculated and plotted according to the absorbance values. Three replicate wells were used to determine each point. The IC_{50} values were calculated using *SPSS* version 22.0.

Annexin V-FITC/PI Apoptosis Analysis

To explore the manner of cancer cell death, the Annexin V-FITC/PI staining assay (Abcam Apoptosis Detection Kit; ab214663) was conducted to assess the percentage of apoptotic SF767 cancer cells according to the manufacturer's instructions.[13] In brief, the SF767 cells were seeded in 6-well plates (1 × 10^6 cells $well^{-1}$) at 37°C and 5 % CO_2 overnight. After the cells grew to the log[illegible]mic stage with a confluence of 70–80 %, nano **1–3** at the concentrations described above were added and the cells incu[illegible]ed for 24 h at 37°C, 5 % CO_2. A negative control was set to DMSO, and cisplatin, known as an apoptosis inducer, was selected as the positive control. After incubation, the cells were collected with 0.25 % w/v trypsin and washed three times with pre-cooled PBS. Annexin V binding buffer (500 μL) was added to re-suspended the SF767 cells followed by 5 μL of Annexin V-FITC and 5 μL of propidium iodide (PI) and 15 min incubation at 37°C in the dark. Finally, the SF767 cells were analysed by flow cytometry (BD Via, New Jersey, USA) for the proportion of intact live cells and apoptotic cells. Three parallel experiments were carried out to reduce the error.

Intracellular ROS Assay

To measure the intracellular ROS generation and accumulation in SF767 cancer cells after treatment with nano **1–3**, the 2,7-dichlorodihydrofluorescein diacetate (DCFH-DA) staining method and flow cytometer were used in this experiment.[14] The results of flow fluorescence reflects the content of intracellular ROS. SF767 cells were planted in 6-well plates (5 × 10^5 cells $well^{-1}$) and incubated at 37°C, 5 % CO_2. When the cells had grown to the logarithmic stage and reached a confluence of 70–80 %, nano **1–3** was added at the concentrations described above. After incubation for 24 h, the cells were harvested with 0.25 % trypsin and detected with a flow cytometer (BD Via, New Jersey, USA) at an excitation wavelength of 488/530 nm. *FlowJo7.6* software was used to analyse the experimental data. All experiments were performed at least three times.

Quantitative Reverse Transcription Polymerase Chain Reaction (qRT–PCR) Assay

The mRNA expression of ROS related genes in SF767 cancer cells after treatment with nano **1–3** was measured using

qRT–PCR according to the published protocol.[15,16] Total RNA in SF767 cancer cells was extracted using a TRIzol Plus RNA Purification Kit (Invitrogen, Carlsbad, CA, USA) according to the instructions, and then the quality of RNA was evaluated using the OD260/OD280 ratio. The cDNA was synthesised using a High-Capacity cDNA Reverse Transcription Kit (Applied Biosystems, Cambridge, MA, USA). The PCR primer sequences in this experiment are listed in Table 2. The PCRs were conducted using a qRT–PCR miRNA Detection Kit (Invitrogen) at 95°C for 15 min, followed by 40 cycles of denaturation at 95°C for 5 s, annealing at 55°C for 30 s, and extension at 72°C for 30s. Each experiment was performed in triplicate and the relative quantification was analysed by the $2^{-\Delta\Delta Ct}$ method.

Table 2. The sequence of primers

Name	Sequence
racl1	CCTGCTCATCAGTTACACGACCA TGTCCCATAGGCCCAGATTCA
gp91	CTTCACACGGCCATTCACAC GTCATAGGAGGGTTTCCGGC
gp22	GACGCTTCACGCAGTGGTACT CACGACCTCATCTGTCACTGG
Gapdh	AATGGGCAGCCGTTAGGAAA GCGCCCAATACGACCAAATC

Data Analysis via the Statistical Method

All the experimental data were expressed in the form of mean ± standard deviation (s.d.) from three parallel experiments. Comparisons between groups were conducted with *Prism* software (version 6.07, GraphPad Software Inc., San Diego, CA).

Results and Discussion

*Crystal Structure of Compounds **1–3***

HL_1 could be produced by the reaction of 2-(piperazin-1-yl) ethan-1-amine with 3-methoxysalicylaldehyde in MeOH solution via reflux in high yield (Scheme 1). Upon slow evaporation of the filtrate, blue block-shaped crystalline products of **1** were formed after one week. The X-ray single crystal structure determination reflects that complex **1** belongs to the space group *C*2/*c* of the monoclinic system and reveals a discrete mononuclear Cu^{II}-based structure. The asymmetrical unit of complex **1** consists of a crystallographically unique Cu^{II} ion, a fully deprotonated L_1^- ligand, and a coordinating AcO^- group, resulting in a charge-neutral structure (Fig. 1). The coordinated environment of the Cu1 atom is completed by three O atoms from one L_1^- ligand and one coordinated AcO^- group along with two N atoms from the L_1^- ligand, shaping the square-planar coordination geometry (Fig. 1b). The bond distances are in the range of 1.891(3) to 1.95[illegible] Å for the Cu^{II}–O bonds and 1.892(4) and 2.038(4) Å for the C[illegible]–bonds, which all locate in the normal range of Cu^{II}–N and Cu^{II}–O bond lengths in Cu^{II}-based

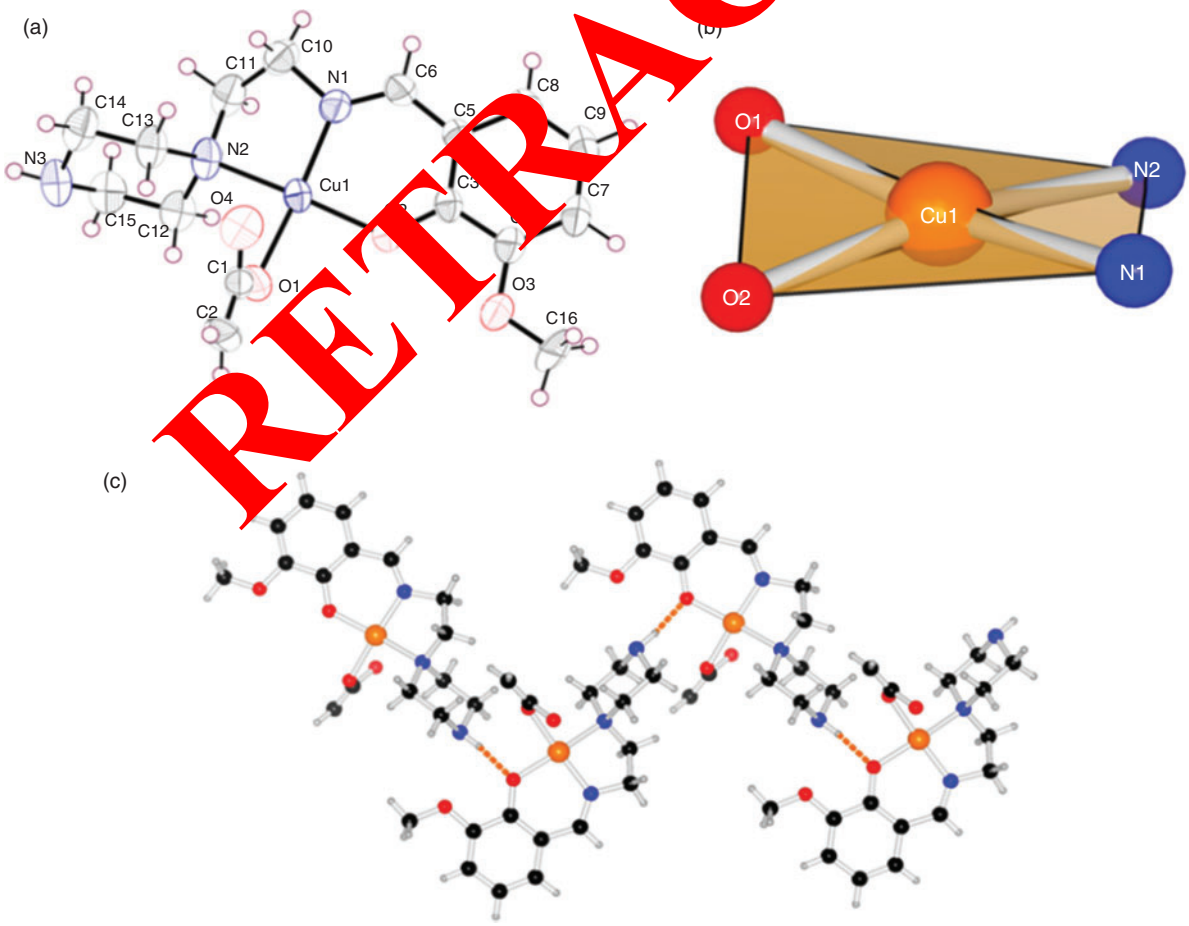

Fig. 1. (a) The chemical drawing for the molecular unit of **1**. (b) The square-planar coordination surroundings for the Cu1 ion. (c) View for the 1D H-bond network of **1**.

coordination complexes reported in the literature.[17,18] The AcO^- group is monodentate chelating with the central Cu^{II} ion while the other O atom forms a weak Cu–O interaction with a distance of 2.633(2) Å. The pyrazine group is in a chair-like conformation, which is far away from the axis position of the square-planar Cu^{II} centre. The discrete mononuclear Cu^{II}-based structure of **1** is further extended into a 1D H-bond network via the H-bond interaction of the N3–H3···O2 (distance: 2.105 Å, Fig. 1c). The formed 1D H-bond network is further packed in the three-dimensional direction to give rise to a 3D supramolecular structure with no π–π interactions.

HL_2 could be produced via the reaction of 2-hydroxy-3-methoxy benzaldeyhde with *N*,*N*-dimethylethane-1,2-diamine in MeOH solution via reflux in a moderate yield. Upon slow evaporation of the filtrate after several days, crystalline products of complexes **2** and **3** were obtained. Complexes **2** and **3** have been characterised by TGA analysis and EA along with the X-ray single crystal analysis. A single crystal X-ray structural determination shows that complex **2** belongs to the space group *Pbca* of an orthorhombic system and shows a discrete binuclear cluster-based structure. The basic molecular unit of **2** is composed of a crystallography unique Co^{II} ion, one coordinated AcO^- group along with one L_2^- ligand. The distorted square-pyramidal coordinated surrounding of the Co^{II} atom is shaped by two N donors from the L_2^- ligands and one O atom from another different L_2^- ligand along with two bridging oxygen atoms from two symmetry-related acetate molecules (symmetrical code: $1 - x$, $1 - y$, $1 - z$, Fig. 2a). The bond distances vary from 1.891(3) to 1.953(3) Å for the Co^{II}–O bonds and are in the region of 1.928(3) and 2.387(2) Å for the Co^{II}–N bonds, which all locate in the normal range of Co^{II}–N and Co^{II}–O bond lengths in other reported Co^{II}-based coordination complexes.[19] Two acetate ions located in the inversion centre chelate with two symmetry-related Co^{II} atoms to shape a dimer unit, and the Co^{II}–Co^{II} separation is 3.442(3) Å. The molecules of **2** are extended into a 1D ladder-like network via C8–H8···O4 H-bond interactions along the *c*-axis with a distance of 2.281(2) Å (Fig. 2b).

Complex **3** was obtained via a slightly modified preparation method of complex **2** via the replacement of $Co(OAc)_2{\cdot}4H_2O$ with $Cu(NO_3)_2{\cdot}3H_2O$ and using NaN_3 as the additive. Structural analysis of **3** via the structural solution and refinement results from the X-ray diffraction data shows that complex **3** locates in the *P*-1 space group of a triclinic system which demonstrates a similar structure to complex **2** which exhibits a binuclear cluster-based structure. The molecular structure has been depicted in Fig. 3a and is made up of two asymmetric units (Z = 2). The binuclear complex is built up of two mononuclear $[CuL_2N_3MeOH]$ moieties linked through azide nitrogen and MeOH oxygen atoms to the central Cu^{II} ions (Fig. 3a). The distorted octahedral coordinated surrounding of the Cu^{II} centre

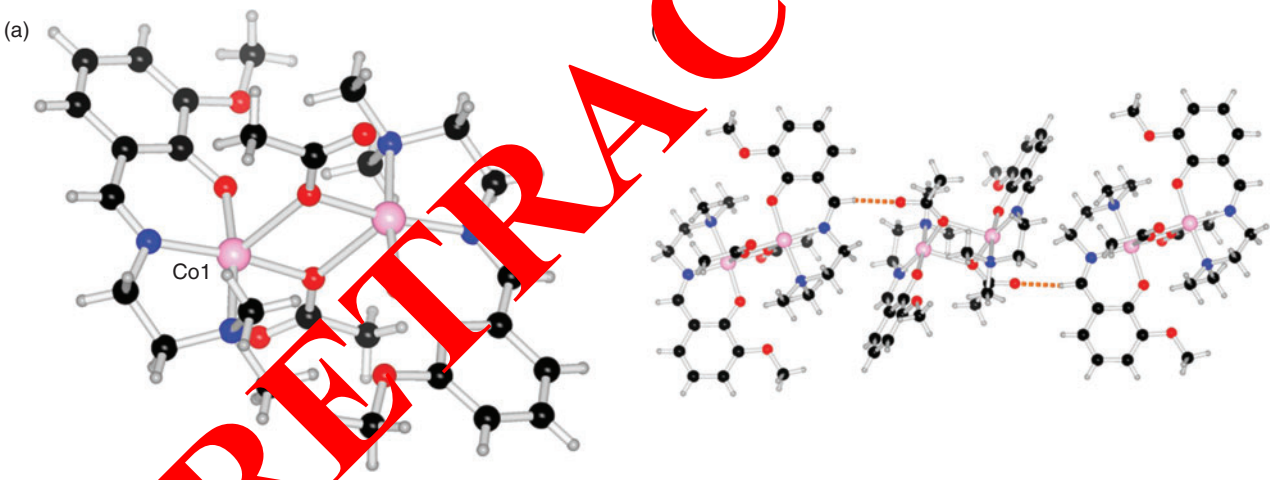

Fig. 2. (a) View for the binuclear Co^{II} molecular structure of **2**. (b) The 1D H-bond network of **2**.

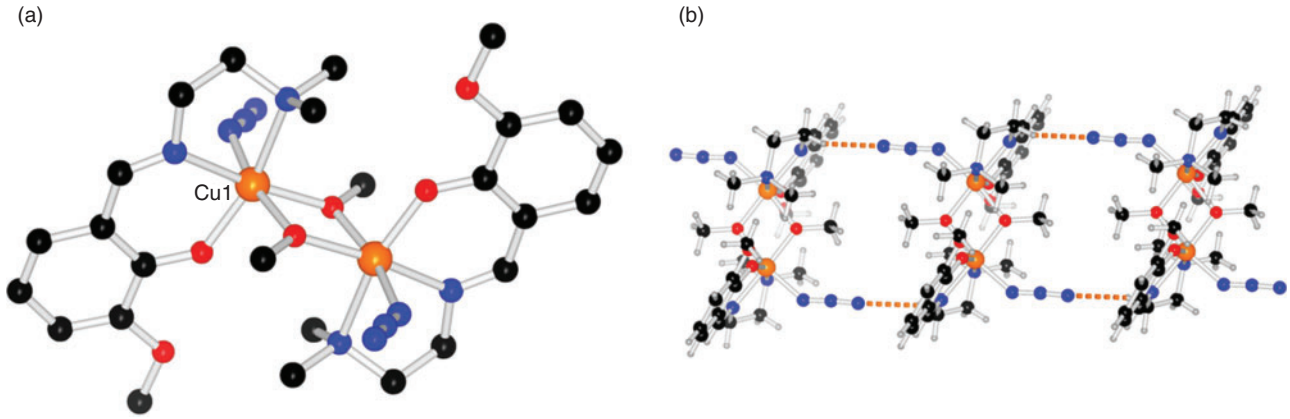

Fig. 3. (a) View for the trinuclear Cu^{II} molecular structure of **3**. (b) The non-classic H-bond interaction between two adjacent discrete structures.

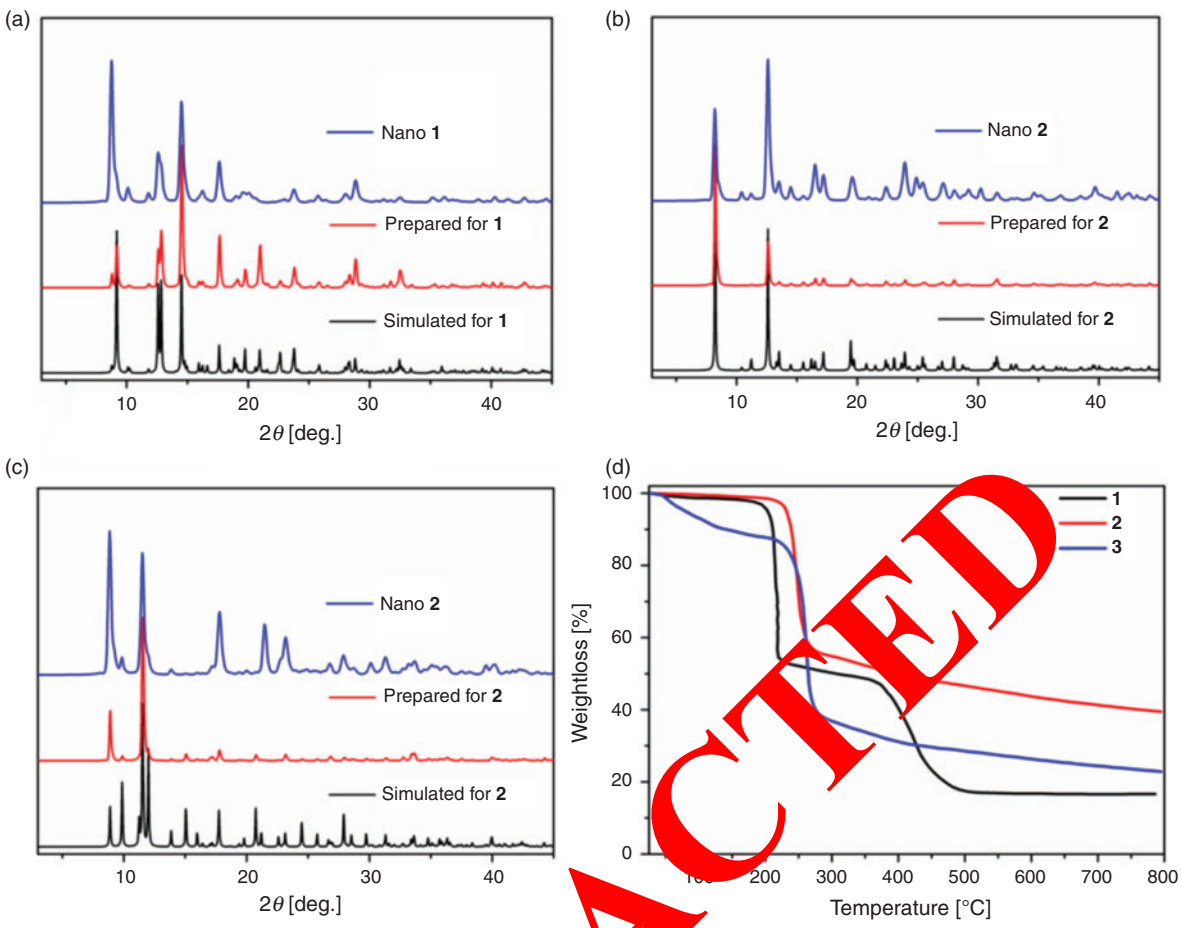

Fig. 4. The PXRD patterns for (a) **1**, (b) **2**, and (c) **3**. (d) TGA curves for complexes **1**–**3**.

is shaped by two nitrogen atoms from the L_2^- ligand and one of the N_3^- group, one O atom from another adjacent L_2^- ligand along with two bridging oxygen atoms from symmetry-related MeOH molecules (symmetrical code: 1 − x, 1 − y, −z). The bond distances are in the range of 1.940(3) to 2.016(3) Å for the Cu^{II}–O bonds and 2.028(4) to 2.029(3) Å for the Cu^{II}–N bonds, which all locate in the normal range of Cu^{II}–O and Cu^{II}–N bond distances in other reported Cu^{II}-based coordination complexes.[15,16] The molecules of **3** are extended into a 1D chain-like structure along the *b*-axis by C10–H10A···N5 H-bond interactions with a distance of 2.592(3) Å (Fig. 3b).

PXRD, TGA, and Nanosizing of Compounds 1–3

To probe the purity of the prepared crystalline compounds **1**–**3**, PXRD curves were collected at ambient temperature. As shown in Fig. 4a–c, the PXRD patterns of the as-prepared three complexes reveal sharp peaks, indicating their high crystallinity. Furthermore, the well matched peak positions of the PXRD patterns between the as-prepared samples and the simulated patterns confirm that the structure of the three complexes match well with their crystal structure. To study the thermal stability and compositions of the lattice solvents, the TGA curves for compounds **1**–**3** were measured in the temperature range of 25 to 800°C under N_2 atmosphere (Fig. 4d). The TGA curve of **1** shows that it could be thermally stable up to 201°C without obvious weight loss, which is consistent with the information observed from the X-ray data. Above 201°C, the sharp weight loss corresponds to the complete decomposition of **1**. For complex **2**, the TGA profile reveals that no obvious change can be found from 25 to 216°C, which indicates that there is no solvent in its crystal lattice, and this agrees with the observation from the crystal data analysis. It should be noted that complex **2** shows a higher framework decomposition temperature than that of complex **1**, which might be attributed to the formation of the binuclear cluster-based structure. For complex **3**, a weight loss of 10.1 % could be observed from 48 to 174°C, corresponding to the loss of one coordinated MeOH molecule. After 216°C, a sharp weight loss can be found, which could be ascribed to the complete decomposition of the complex.

In preparation for the CCK-8 assay, used for the evaluation of the cytotoxicity towards the cancer cell lines, nano-sized particles of compounds **1**–**3** were desired, which could allow them to pass though the cell membrane more easily and reach the regions of issue in the whole body by injection.[20] Previous literature has reported that mechanical grinding could be used to produce nanosized coordination complexes without further chemical manipulation.[21] To reduce the size of the crystalline complexes **1**–**3** to the nanoscale region, a ball mill was applied to grind the samples for ~30 min. The crystalline nature of the samples was checked by a comparison of the PXRD patterns of the simulated and the ground samples, which revealed that they show a good match with each other. The successful formation of the coordination nanoparticles was also confirmed by the significant broadening of the peaks of the ground samples.[22] The particle size and morphology of the formed nano coordination complexes were validated via SEM measurements obtained by

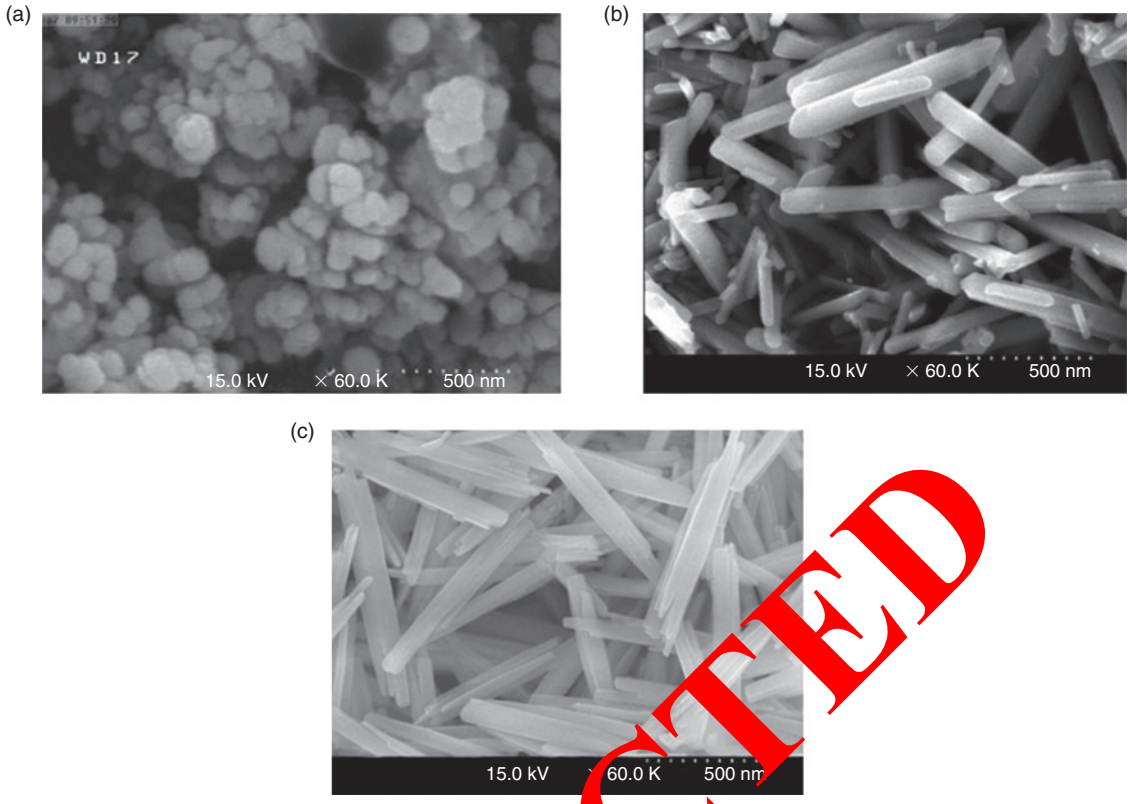

Fig. 5. The SEM images of com es (a) **1**, b) **2**, and (c) **3**.

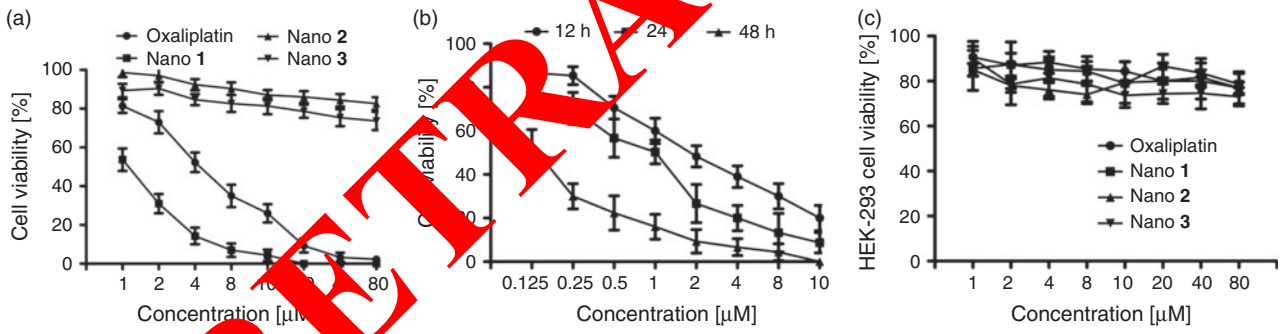

Fig. 6. The viability d prol ration of SF767 cancer cells after treatment with the indicated concentrations of nano **1–3**. (a) The cell viability curves of SF767 cancer cells mea d and ed by the CCK8 method after treatment with significant doses of nanoparticles for 24 h. (b) The time dependent relationship of nano **1** on SF cancer viability and proliferation. (c) All the nano **1–3** showed no cytotoxicity on normal human HEK293 cells after treatment with various doses for 24 h. D represent mean ± s.d. All experiments were performed in triplicate.

drop-casting ground samples of **1–3** dispersed in DMSO on a glass surface (Fig. 5). Nano **2** and **3** adopt almost a nanorod type morphology with average widths of 680 and 446 nm and a thickness of 280 and 170 nm, respectively. It is also interesting to note that the nanorods have a very smooth surface and their tips split into several much smaller nanorods. In comparison, nano **1** exhibits a spherical type morphology with an average size of 70 nm.

*Anti-Proliferation Activity of Nano **1–3** against SF767 Cancer Cells*

To detect the anticancer effect of nano **1–3** on human intracranial aneurysm SF767 cell viability and proliferation, a CCK8 detection kit was used. Serially diluted nano **1–3** was incubated with SF767 cancer cells for 24 h at different dilutions. The negative control was set to DMSO with oxaliplatin as the positive control drug. As results show in Fig. 6, nano **1** decreased SF767 cancer cell viability in a concentration-dependent manner, and nano **2**

Table 3. **IC_{50} values of nano 1–3**

Cell	Drug IC_{50} value[A] [mM]			
	Nano **1**	Nano **2**	Nano **3**	Oxaliplatin
SF767	1.0 ± 0.01	>80	>80	4.8 ± 0.2
HEK-293	>80	>80	>80	>80

[A]The IC_{50} values were calculated according the cell viability curves presented in Fig. 6. Each value is shown as mean ± s.d. of three independent experiments.

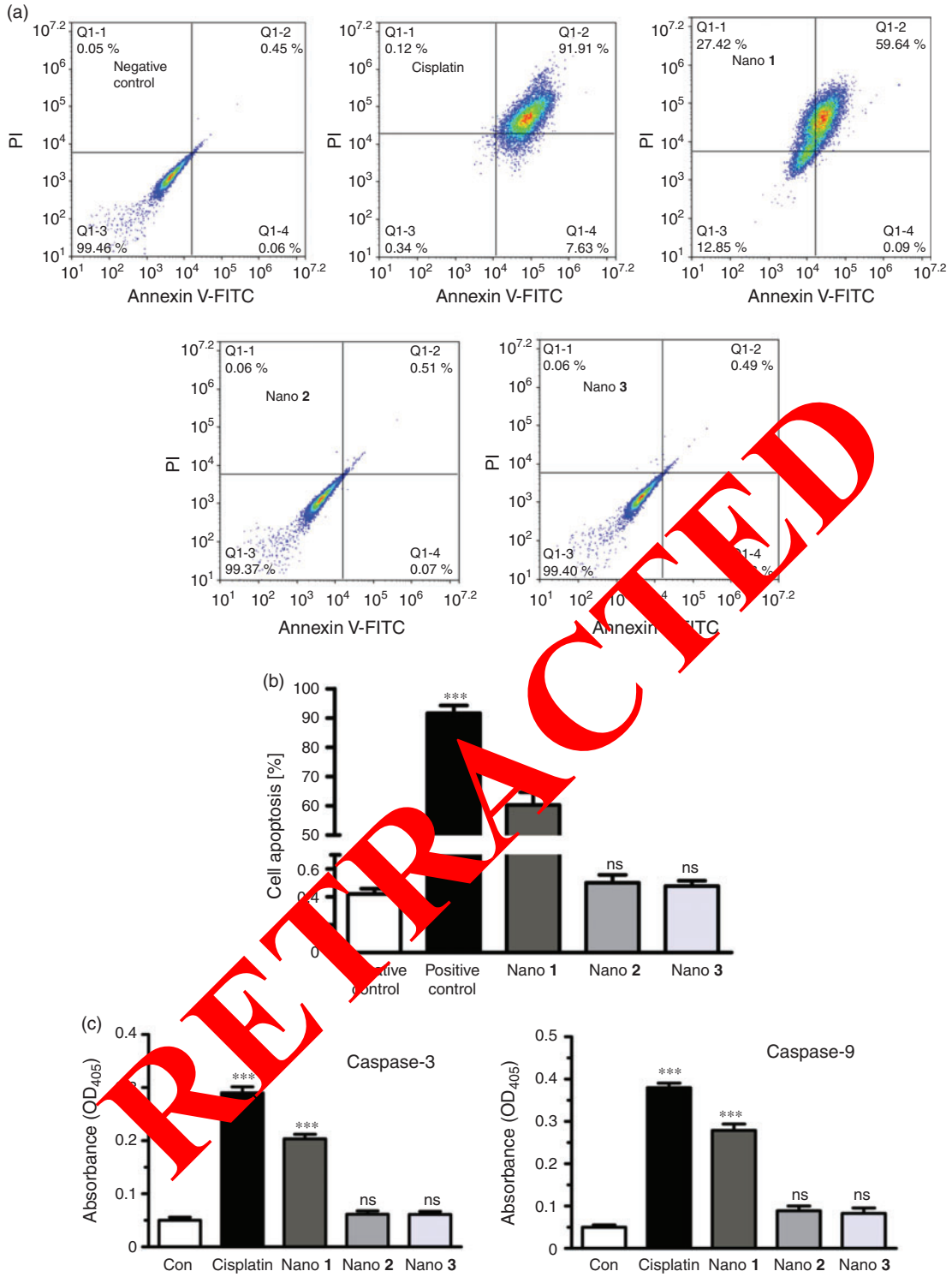

Fig. 7. SF767 cancer cell apoptosis detected using the Annexin V-FITC/PI double staining method. The apoptotic SF767 cancer cells were detected by flow cytometer combined with Annexin V-FITC/PI double staining. The cells were exposed to nano **1–3** at the indicated doses, the solvent and cisplatin were used as the negative and positive control drug (a). The statistical results of Fig. 7a (b). The activation level of caspase 3 and caspase 9 under nano treatment (c).

and **3** had no inhibitory effect on SF767 cancer cell viability (Fig. 6a). The inhibition effect of nano **1** on SF767 cancer cells also showed a time-dependent relationship (Fig. 6b). In addition to this, nano **1**–**3** showed no effect on the viability and proliferation of the normal human HEK293 cells (Fig. 6c).

The IC_{50} values were calculated according to the SF767 cancer cell viability curves with *SPSS 22.0*, and the detailed data are listed in Table 3. Nano **1** exhibited extraordinary anti-proliferation activity on SF767 cells with an IC_{50} value of 1.0 ± 0.01 μM. However, nano **2** and **3** had IC_{50} values of over

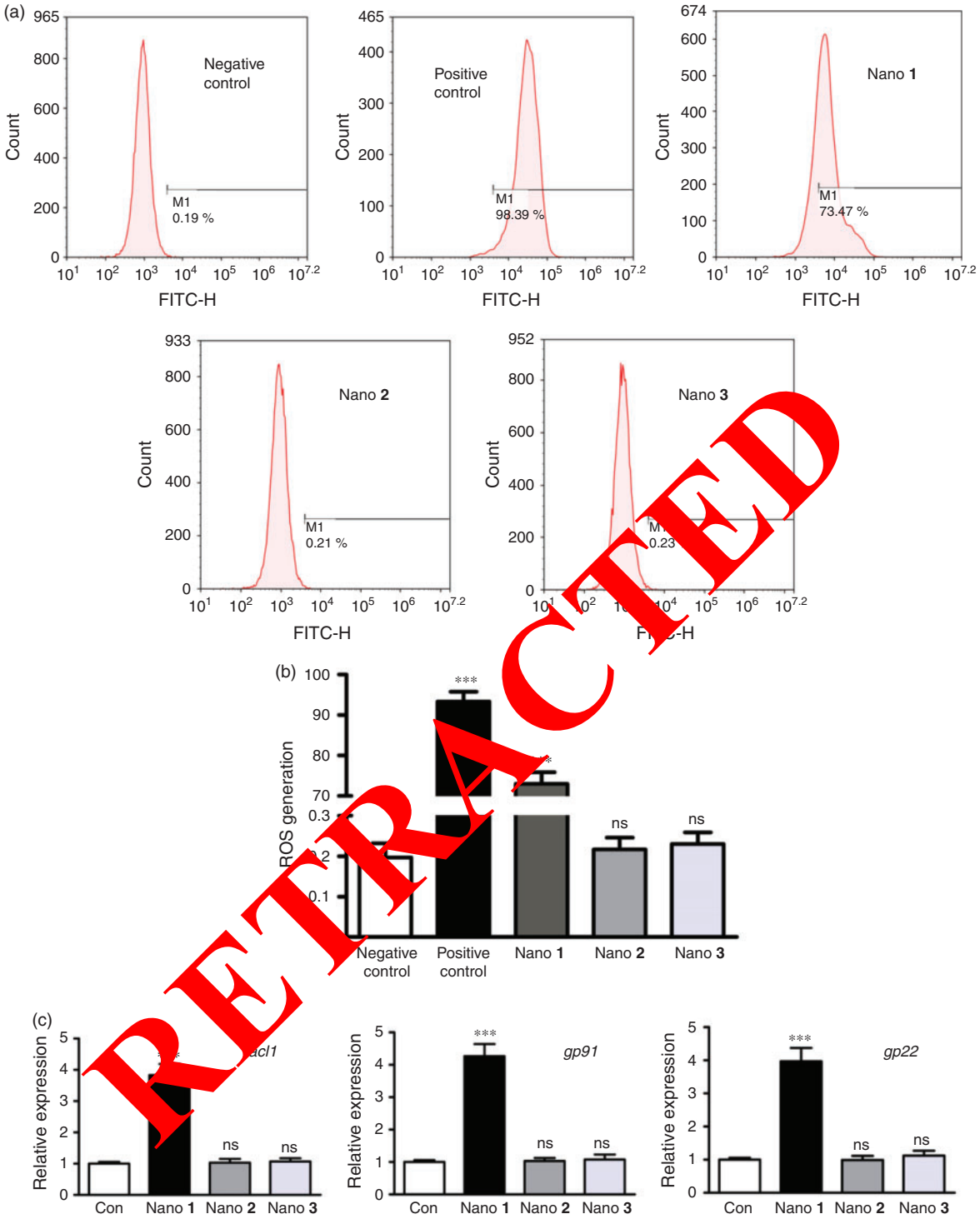

Fig. 8. Nano **1** initiates intracellular ROS generation and accumulation. The ROS content in SF767 cancer cells was quantified by flow cytometry after treated with nano **1–3** at the indicated doses. The solvent and cisplatin were used as the control drug (a). Statistical results of ROS production in each group (b). The expression of ROS related genes in each group (c).

80 μM. This indicates that nano **1** has potential implications for human intracranial aneurysm treatment.

*Nano **1** Induces Apoptotic Cell Death*

The manner of cell death of SF767 cancer cells caused by nano **1–3** was investigated by an Annexin V-FITC/PI double staining assay. Cisplatin, an apoptosis inducer, was used as the positive treatment. As the results show in Fig. 7a, treatment with nano **1** ($1 \times IC_{50}$) significantly increased the rate of apoptotic cells to 59.64 ± 1.52 %. In accordance with the CCK8 detection results, nano **2** and **3** could not induce apoptotic cell death in SF767 cancer cells.

Cleaved caspase-3 and cleaved caspase-9 are the key markers of cell apoptosis, its activation was detected by a Caspase

Colourimetric Protease Assay Sampler Kit (Fig. 7c). From the results, we can see that nano **1** could induce the activation of capase-3 and caspase-9 significantly, while the caspase activation had no change under the treatment of nano **2** and **3**. Together, these data indicated that nano **1** stimulated a loss in cell viability via cell apoptosis, which was associated with activation of caspase 3 and 9.

*Nano **1** Induces Intracellular ROS Generation and Accumulation*

A previous study had reported that mitochondrial dysfunction is a key factor in apoptotic cell death. Therefore, we speculated that mitochondrial dysfunction lead to increased ROS and finally induced the SF767 cancer cell apoptosis under the treatment of nano **1**. The ROS production in SF767 cancer cells was determined via flow cytometry. Compared with nano **2** and **3**, nano **1** ($1 \times IC_{50}$) could significantly increase the intracellular ROS level in SF767 cancer cells to the percentage of $73.47 \pm 2.8\,\%$ (Fig. 8). These data confirm that nano **1** could cause apoptotic cell death in SF767 cancer cells via increasing the ROS accumulation in cells.

Crystallographic Data

CCDC Nos 1896855–1896857 contain the supplementary crystallographic data for this paper. These data can be obtained free of charge from The Cambridge Crystallographic data Center via http://www.ccdc.cam.ac.uk/data_request/cif.

Conclusion

In summary, three novel trinuclear Schiff base transition metal (II) complexes based on two newly designed Schiff base ligands have been successfully prepared via the solvent volatilisation method. The as-prepared three complexes were characterised using various physicochemical techniques, e.g. SCXRD, EA, PXRD, and TGA. Furthermore, the particle sizes of these coordination complexes have been successfully reduced to the nano-region via a hand grinding method. In addition, the anti-tumour activity of nano **1**–**3** was explored. The anti-proliferation effect of nano **1**–**3** was evaluated on a human SF767 cell line. CCK-8 results indicated that only nano **1** has excellent anticancer activity on SF767 cells, and this inhibitory effect shows a dose and time independent relationship with nano **1**. Mechanism investigations revealed that nano **1** induces the SF767 cell death via the classical (caspase 3 and 9 dependent) apoptosis pathway. In addition, we revealed that the caspase pathway is initiated by the increased accumulation of intracellular ROS.

Conflicts of Interest

The authors declare no conflicts of interest.

Acknowledgements

The research did not receive any specific funding.

References

[1] A. Jemal, F. Bray, M. M. Center, J. Ferlay, E. Ward, D. Forman, *CA Cancer J. Clin.* **2011**, *61*, 69. doi:10.3322/CAAC.20107

[2] N. Etminan, G. J. Rinkel, *Nat. Rev. Neurol.* **2016**, *12*, 699. doi:10.1038/NRNEUROL.2016.150

[3] R. D. Brown, J. P. Broderick, *Lancet Neurol.* **2014**, *13*, 393. doi:10.1016/S1474-4422(14)70015-8

[4] N. Alvarez, L. F. S. Mendes, M. G. Kramer, M. H. Torre, A. J. Costa-Filho, J. Ellena, G. Facchin, *Inorg. Chim. Acta* **2018**, *483*, 61. doi:10.1016/J.ICA.2018.07.052

[5] A. C. Hangan, G. Borodi, R. L. Stan, E. Páll, M. Cenariu, L. S. Oprean, B. Sevastre, *Inorg. Chim. Acta* **2018**, *482*, 884. doi:10.1016/J.ICA.2018.07.045

[6] P. Sukanya, C. Venkata Ramana Reddy, *Appl. Organomet. Chem.* **2018**, *32*, e4526. doi:10.1002/AOC.4526

[7] K. Skalsky, D. Yahav, A. Lazarovitch, N. Eliakim-Raz, L. Leibovici, M. Paul, *Clin. Microbiol. Infect.* **2012**, *18*, 370. doi:10.1111/J.1469-0691.2012.03838.X

[8] D. S. Raja, N. S. P. Bhuvanesh, K. Natarajan, *Dalton Trans.* **2012**, *41*, 4365. doi:10.1039/C2DT12274J

[9] C. Vidya Raj, M. P. Kesharwani, G. G. Vinoth Kumar, M. J. D. Jeyaraj, J. Rajesh, K. Rajagopal, *Appl. Organomet. Chem.* **2018**, *32*, e4538. doi:10.1002/AOC.4538

[10] W. Jian, X. Tang, C. Z. Xie, H. Tian, X. Q. Song, H. T. Pan, Y. Qiao, J. Y. Xu, *Dalton Trans.* **2016**, *45*, 9073. doi:10.1039/C6DT00461J

[11] A. Revathi, M. Sankarganesh, J. Rajesh, J. D. Raja, *J. Fluoresc.* **2017**, *27*, 801. doi:10.1007/S10895-017-2118-Y

[12] Y. B. Zheng, G. C. Xiao, S. L. Tong, Y. Ding, Q. S. Wang, S. B. Li, Z. N. Hao, *World J. Gastroenterol.* **2015**, *21*, 7197. doi:10.3748/WJG.V21.I23.7197

[13] G. Xie, Q. Ke, Y. Z. Ji, A. Q. Wang, M. Jing, L. L. Zou, *Braz. J. Med. Biol. Res.* **2018**, *52*, e7816. doi:10.1590/1414-431X20187816

[14] Z. Wang, H. Luo, H. Xia, *Mol. Med. Rep.* **2018**, *18*, 3791. doi:10.3892/MMR.2018.9352

[15] E. Mfotie Njoya, J. N. Eloff, L. J. McGaw, *BMC Complement. Altern. Med.* **2018**, *18*, 305. doi:10.1186/S12906-018-2372-9

[16] P. Zhang, S. Li, C. Lv, J. Si, Y. Xiong, L. Ding, Y. Ma, Y. Yang, *Theranostics* **2018**, *8*, 5890. doi:10.7150/THNO.27667

[17] İ. Gönül, A. Burak, S. Karaca, O. Şahin, S. Serin, *Inorg. Chim. Acta* **2018**, *477*, 75. doi:10.1016/J.ICA.2018.02.026

[18] T. Maity, D. Saha, S. Bhunia, P. Brandão, S. Das, S. Koner, *RSC Adv.* **2015**, *5*, 82179. doi:10.1039/C5RA14758A

[19] M. X. Zheng, X. J. Gao, C. L. Zhang, L. Qin, H. G. Zheng, *Dalton Trans.* **2015**, *44*, 4751. doi:10.1039/C4DT04011B

[20] X. Du, R. Fan, L. Qiang, K. Xing, H. Ye, X. Ran, Y. Song, P. Wang, Y. Yang, *ACS Appl. Mater. Interfaces* **2017**, *9*, 28939. doi:10.1021/ACSAMI.7B09227

[21] S. Mukherjee, S. Ganguly, K. Manna, S. Mondal, S. Mahapatra, D. Das, *Inorg. Chem.* **2018**, *57*, 4050. doi:10.1021/ACS.INORGCHEM.8B00237

[22] B. Mirtamizdoust, B. Shaabani, A. Khandar, H. K. Fun, S. Huang, M. Shadman, P. Hojati-Talemi, *Z. Anorg. Allg. Chem.* **2012**, *638*, 844. doi:10.1002/ZAAC.201100492